Neutron Diffraction and Molecular Dynamics Study of Liquid Benzene and Its Fluorinated Derivatives as a Function of Temperature

M. Isabel Cabaço*

Centro de Física da Matéria Condensada UL, Av. Prof. Gama Pinto 2, 1699 Lisboa Codex, Portugal, and Departamento de Física, Instituto Superior Técnico, Av. Rovisco Pais, 1096 Lisboa, Portugal

Yann Danten and Marcel Besnard

Laboratoire de Spectroscopie Moléculaire et Cristalline, CNRS (URA 124), Université de Bordeaux I, 351, Cours de la Libération, 33405 Talence Cedex, France

Yves Guissani and Bertrand Guillot

Laboratoire de Physique Théorique des Liquides, CNRS (URA 765), Université Pierre et Marie Curie, 75252 Paris Cedex, France

Received: April 17, 1997; In Final Form: June 12, 1997[⊗]

The study of the local translational and orientational ordering in benzene (C_6H_6), 1,3,5-trifluorobenzene ($C_6H_3F_3$) and hexafluorobenzene (C_6F_6) neat liquids has been performed along their liquid−vapor coexistence curve between the melting point and the boiling point combining neutron diffraction experiments and molecular dynamics simulation. Both experiment and simulation show that the local ordering is only very slightly affected in the temperature range investigated. The analysis of the results show that the orientational local order in liquid benzene is almost isotropic at distances corresponding to the first shell of neighbors. In contrast, for hexafluorobenzene, parallel and perpendicular configurations exhibit maxima of occurrence for distinct *r* values, parallel configurations being predominant at short distances. For 1,3,5-trifluorobenzene, the orientational order in the first shell is strongly anisotropic, and a stacked configuration involving a pair of molecules is observed at short distances (about 4 Å). This finding together with the value of the coordination number obtained from simulation data clearly shows the existence of dimers (sandwichlike). Finally it is argued that the orientational and translational ordering observed in the hexafluorobenzene is intermediate between those of benzene and those of 1,3,5-trifluorobenzene.

I. Introduction

Recently, we have performed a structural investigation of liquid cyclopropane composed of the simplest cyclic, organic molecules (having a D_{3h} symmetry).[1] The results have prompted us to carry on a new study aimed at probing the evolution of the local order in simple organic liquids constituted of nonflexible cyclic molecules such as benzene and its fluorinated derivatives. The structure of liquid benzene has been extensively studied by X-rays[2] and neutron diffraction[3−6] and also by computer simulations[7−11] as well. However, let us emphasize that most of these investigations have been done in a restricted temperature range close to room temperature, probably as small changes are expected.

The choice of the fluorinated derivatives, namely hexafluorobenzene (C_6F_6) with a D_{6h} symmetry and 1,3,5-trifluorobenzene ($C_6H_3F_3$) with a D_{3h} symmetry deserves some comments. Indeed, it is well established that the structure of a liquid is primarily governed by the short-range forces (in a pictorial way, by the shape of the molecules). The fluorinated derivatives have shapes similar to the benzene one, and therefore it may be expected that the local ordering in the three liquids should not be drastically different. However, the electrostatic interactions could also play a role in the orientational correlations. For instance, for a pair of benzene molecules, the quadrupole−quadrupole interactions favor configurations where the main symmetry axes of the molecules are perpendicular.[12] This is the situation existing in the liquid phase, where perpendicular configurations have been put in evidence.[2−6] In the same way, liquid hexafluorobenzene which is composed of molecules having a quadrupolar moment (3.2×10^{-39} C m^2) similar in magnitude to the benzene one (-2.9×10^{-39} C m^2), but with an opposite sign, also displays a structure where perpendicular configurations seems to be favored.[3,4] In contrast, the quadrupole moment of 1,3,5-trifluorobenzene is small (0.32×10^{-39} C m^2) as compared with the previous ones, and therefore the contribution of higher multipole moments, in particular the octopole one, is not negligible. This last conclusion is supported by far-IR spectroscopic studies of the three liquids which have shown that it is only for liquid 1,3,5-trifluorobenzene that the spectrum cannot be interpreted in the frame of a quadrupole-induced dipole mechanism.[13,14] Hence, it might be inferred from all these considerations that the structure of liquid 1,3,5-trifluorobenzene should be different from the previous ones.[15]

As noted previously structural investigations on liquid benzene combining neutron diffraction and molecular dynamics simulations to study the evolution of the local ordering along the liquid−vapor coexistence curve (from temperatures close to the melting point up to the boiling point) have not been reported so far. Similarly, for hexafluorobenzene only measurements combining X-rays and neutron diffraction have been reported at room temperature.[3,4] The only available and indirect structural information concerning the temperature dependence

* Corresponding author. E-mail: isabel@alf1.cii.fc.ul.pt. Fax: 351 1 7954288.

[⊗] Abstract published in *Advance ACS Abstracts,* August 1, 1997.

S1089-5647(97)01331-X CCC: $14.00

of the local ordering for these two liquids has been obtained from the integrated intensity of depolarized light scattering.[16,17] It was found that a transition between local structures generated by dimers could be detected in both neat liquids. In contrast high-resolution stimulated Brillouin gain spectroscopy measurements show no evidence of "structural transition".[18] Such behavior is rather unusual and merits being investigated further using the diffraction technique. Finally, as far as we know, the structure of liquid 1,3,5-trifluorobenzene has not been reported.

For all these reasons, we have decided to study the local ordering and its evolution as a function of the temperature for these three molecular neat liquids. We will follow here the approach previously used and based on the analysis of neutron diffraction results with the help of molecular dynamics simulations.[1] This study also constitutes the first necessary step toward the understanding of the structure of binary mixtures of benzene and its two fluorinated derivatives, which will be presented in a forthcoming paper.[19]

II. Theoretical Background

In a neutron diffraction experiment the total differential cross section per molecule $(\partial\sigma/\partial\Omega)_{\text{total}}$ is the sum of a coherent and an incoherent contribution:

$$\left(\frac{\partial\sigma}{\partial\Omega}\right)_{\text{total}} = \left(\frac{\partial\sigma}{\partial\Omega}\right)^{\text{coh}} + \left(\frac{\partial\sigma}{\partial\Omega}\right)^{\text{incoh}} \tag{1}$$

where the coherent contribution is usually separated into a distinct and a self-term.

For a molecular liquid, this distinct coherent contribution involves the coherent scattering due to the distinct nuclei of either different molecules (intermolecular) or the same molecule (distinct intramolecular). Therefore eq 1 can be written as a sum of four contributions:

$$\left(\frac{\partial\sigma}{\partial\Omega}\right)_{\text{total}} = \left(\frac{\partial\sigma}{\partial\Omega}\right)_{\text{intra}}^{\text{dist}} + \left(\frac{\partial\sigma}{\partial\Omega}\right)_{\text{inter}} + \left(\frac{\partial\sigma}{\partial\Omega}\right)^{\text{self-coh}} + \left(\frac{\partial\sigma}{\partial\Omega}\right)^{\text{incoh}} \tag{2}$$

The last two terms in eq 2 give rise to the so-called self-differential cross section:

$$\left(\frac{\partial\sigma}{\partial\Omega}\right)^{\text{self}} = \sum_i (b_i)^2 + \sum_i (b_i^{\text{inc}})^2 \tag{3}$$

where b_i and b_i^{inc} are respectively the coherent and the incoherent scattering lengths of the nucleus i and the sum runs over all the nuclei of the molecule.

The distinct terms are function of the momentum transfer Q defined as

$$Q = (4\pi/\lambda)\sin\theta \tag{4}$$

where 2θ is the scattering angle and λ is the incident neutron wavelength.

The distinct intramolecular contribution can be calculated as

$$\left(\frac{\partial\sigma}{\partial\Omega}\right)_{\text{intra}}^{\text{dist}} = \sum_{i\neq j} b_i b_j j_0(Qr_{ij}) \exp(-{}^1/_2 l_{ij}{}^2 Q^2) \tag{5}$$

where $j_0(Qr_{ij})$ is the spherical Bessel function of zero order; r_{ij} is the distance between the i and j nuclei, and l_{ij} the corresponding root-mean-square fluctuation.

At very large Q values, the intermolecular contribution $(\partial\sigma/\partial\Omega)_{\text{inter}}$ approaches 0, and the relevant contribution to the coherent differential cross section comes from the intramolecular contribution. The asymptotic value (when $Q \rightarrow \infty$) of the $(\partial\sigma/\partial\Omega)^{\text{coh}}$ contribution is the self-coherent differential cross section. On the other hand, when Q approaches zero

$$\lim_{Q\to 0}\left(\frac{\partial\sigma}{\partial\Omega}\right)^{\text{coh}} = (\sum_i b_i)^2 k_{\text{B}} T \rho \chi_{\text{T}} \tag{6}$$

where χ_{T} and ρ are the isothermal compressibility and the number density of the liquid at the temperature T, respectively.

The intermolecular pair correlation function $g_{\text{inter}}(r)$ is obtained from $(\partial\sigma/\partial\Omega)_{\text{inter}}$ as

$$d_{\text{inter}}(r) = 4\pi\rho r[g_{\text{inter}}(r) - 1] = \frac{2}{\pi}\int_0^\infty Q \frac{(\partial\sigma/\partial\Omega)_{\text{inter}}}{(\sum_i b_i)^2} \sin(Qr)\, \mathrm{d}Q \tag{7}$$

The inverse Fourier transform of eq 7 leads to

$$\frac{1}{(\sum_i b_i)^2}\left(\frac{\partial\sigma}{\partial\Omega}\right)_{\text{inter}} = \frac{4\pi\rho}{Q}\int_0^\infty r[g_{\text{inter}}(r) - 1]\sin(rQ)\, \mathrm{d}r \tag{8}$$

where $g_{\text{inter}}(r)$ is given by

$$g_{\text{inter}} = \sum_{i,j} b_i b_j g_{ij}(r)/(\sum_i b_i)^2 \tag{9}$$

For benzene, hexafluorobenzene and 1,3,5-trifluorobenzene, $g_{\text{inter}}(r)$ is a weighted sum of partial correlation functions $g_{ij}(r)$, namely

$$g(r)_{C_6D_6} = 0.25 g_{CC} + 0.25 g_{DD} + 0.50 g_{CD} \tag{10}$$

$$g(r)_{C_6D_3F_3} = 0.27 g_{CC} + 0.07 g_{DD} + 0.05 g_{FF} + 0.27 g_{CD} + 0.23 g_{CF} + 0.11 g_{DF} \tag{11}$$

$$g(r)_{C_6F_6} = 0.29 g_{CC} + 0.21 g_{FF} + 0.50 g_{CF} \tag{12}$$

Perdeuterated molecules have been used in order to minimize the incoherent contribution for experimental intensities.

III. Experimental and Data Reduction

1. Experimental Setup. The experiments were performed on the two-axes spectrometer 7C2,[20] situated on the hot source of the Orphée reactor at the Laboratoire Léon Brillouin (Laboratoire Commun CEA-CNRS, Saclay, France). The incident neutron wavelength $\lambda = 0.70$ Å was selected by means of a Cu 111 monochromator. The scattered intensities were measured simultaneously with a BF_3 position-sensitive detector containing 640 cells. These cells cover, with a step of 0.2°, an angular range from $0° \leq 2\theta \leq 128°$, hence allowing measurements up to a momentum transfer of $Q \approx 16$ Å^{-1}. The wavelength and detector zero angle were obtained from standard calibration measurements using a nickel powder.

Deuterated benzene (99.95% isotopically enriched in deuterium) and hexafluorobenzene were supplied by Aldrich. The deuterated 1,3,5-trifluorobenzene was synthesized and the isotopic purity (97.8%) was checked using NMR spectrometry. The sample was held in a vanadium cylindrical container (0.1 mm thick) with an internal diameter of 6 mm and was placed in the 45 mm high neutron beam. The cell was mounted in a thermostat and heated from a temperature close to the melting point up to a temperature just below the boiling point (see Table 1). During the runs, the temperature of the sample was kept constant within $\Delta T = \pm 0.2$ K.

TABLE 1: Dependence upon the Temperature of the Density *d* of Liquid Benzene, 1,3,5-Trifluorobenzene, and Hexafluorobenzene (d/kg m^{-3}) (See Text)[a]

T/K	C_6D_6	$C_6D_3F_3$	C_6F_6
271		1343	
282	956		1646
298	939	1296	1606
313			1572
320			1557
323	911	1256	
328			1538
340			1510
345		1220	
348	882		
350			1483
mp/K	278.55	267.65	278.45
bp/K	353.41	348.65	353.65

[a] Melting point (mp) and boiling point (bp) are taken from ref 39.

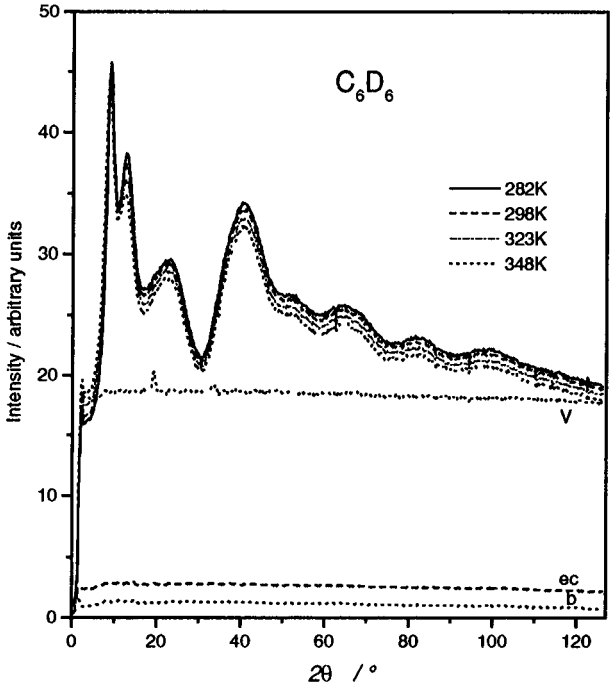

Figure 1. Experimental scattered intensities of liquid benzene C_6D_6 as a function of the temperature. The background (b), vanadium (V), and the empty cell (ec) runs are reported.

Independent measurements of the empty cell, of the background and of a vanadium rod with the same dimensions of the sample, were performed. Several runs were accumulated (typically 10 for the sample and the container, 6 for the vanadium rod and for the background) in blocks of 10^3 monitor counts.

Typical diffraction patterns obtained for liquid benzene and for the empty cell are reported in Figure 1. In this figure, the background and the vanadium runs are also displayed for comparison.

2. Data Reduction. Corrections for background, container scattering, and self-absorption were carried out using conventional methods[21] based upon Paalman and Pings' formalism[22] and for multiple scattering using the isotropic approximation of Blech and Averbach.[23]

The values of the density, as a function of the temperature, have been reported for liquid benzene.[24] For 1,3,5-$C_6D_3F_3$ and C_6F_6 we have calculated the density against temperature using the Rackett equation as modified by Spencer and Danner.[25] Therefore we have assumed here that the molar volumes were the same for the hydrogenated and deuterated compounds, to calculate the densities reported in Table 1.

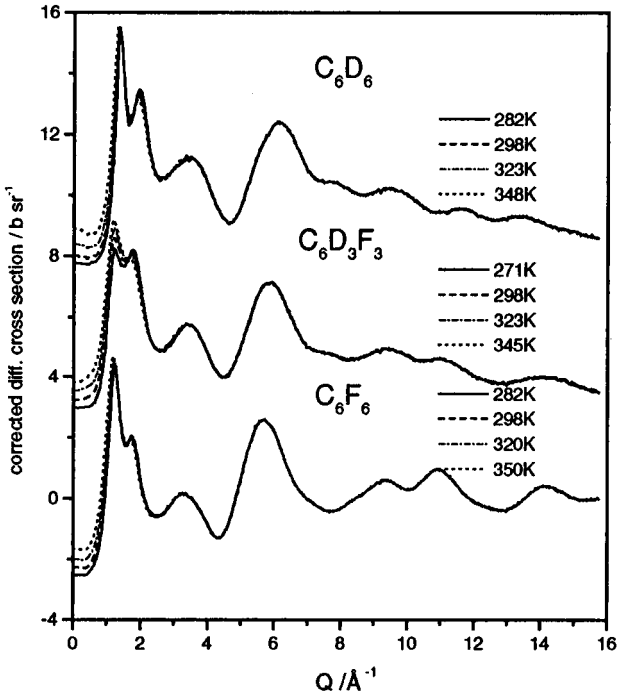

Figure 2. Corrected differential cross sections of liquid C_6D_6, 1,3,5-$C_6D_3F_3$, and C_6F_6 as a function of the temperature. For clarity, curves are shifted: +5 for C_6D_6, −4 for C_6F_6.

The corrected data were then scaled to absolute units using the corrected vanadium intensities as a standard. The corrected differential cross sections of the three neat liquids as a function of the temperature are presented in Figure 2.

It is apparent from this figure that for *Q* values greater than about 4 Å^{-1} the differential cross sections are temperature independent for the three liquids. It appears also from this figure that the inelasticity effects are clearly less marked in C_6F_6 than for the other ones. The inelasticity corrections due to the experimental conditions—energy integration performed at constant scattering angle 2θ and not at constant *Q* values—have been discussed by several authors using different approaches.[21,26−32]

If one takes into account the inelasticity effects, the total differential cross section (eq 2) may be written as

$$\left(\frac{\partial\sigma}{\partial\Omega}\right)_{\text{total}}^{\text{exp}} = \left(\frac{\partial\sigma}{\partial\Omega}\right)_{\text{intra}}^{\text{dist}} + \left(\frac{\partial\sigma}{\partial\Omega}\right)_{\text{inter}} + \left(\frac{\partial\sigma}{\partial\Omega}\right)^{\text{self}}[1 + P(Q)] \quad (13)$$

where inelasticity contributions to the distinct term (intramolecular) have been neglected.

At *Q* values greater than about 5 Å^{-1} for the studied liquids, the contribution of the term $(\partial\sigma/\partial\Omega)_{\text{inter}}$ becomes negligible and eq 13 may be written as

$$\left(\frac{\partial\sigma}{\partial\Omega}\right)_{\text{total}}^{\text{exp}} - \left(\frac{\partial\sigma}{\partial\Omega}\right)_{\text{intra}}^{\text{dist}} - \left(\frac{\partial\sigma}{\partial\Omega}\right)^{\text{self}} = \left(\frac{\partial\sigma}{\partial\Omega}\right)^{\text{self}} P(Q) \quad (14)$$

The coherent distinct cross section $(\partial\sigma/\partial\Omega)_{\text{intra}}^{\text{dist}}$ can be calculated using eq 5 and the parameters reported in Table 2[33−35] (see also next paragraph). The total differential self cross section has been calculated using in eq 3 the tabulated scattering lengths.[36] Finally *P(Q)* has been adjusted (via eq 14) in using an even polynomial form ($P(Q) = A + B\,Q^2 + CQ^4$).

IV. Main Observations

The distinct coherent cross sections $(\partial\sigma/\partial\Omega)^{\text{dist}-\text{coh}}$ obtained after all these corrections are displayed in Figure 3 at the two extreme temperatures investigated and the calculated $(\partial\sigma/\partial\Omega)_{\text{intra}}^{\text{dist}}$ are reported for comparison, as well. In the *Q*

TABLE 2: Molecular Parameters of C_6H_6, $C_6H_3F_3$, and C_6F_6, Distances r_{ij}, and Corresponding Root-Mean-Square Fluctuations l_{ij}[a]

	C_6H_6	$C_6H_3F_3$	C_6F_6
		r_{ij}/Å	
C−C	1.390(1.394)[b]	1.39(1.384)[c]	1.393(1.394)[d]
C−D	1.082(1.084)[b]	1.08(1.069)[c]	
C−F		1.32(1.339)[c]	1.322(1.327)[d]
		l_{ij}/Å	
C_1-C_2	0.04626[b]	0.041[c]	0.03[d]
C_1-C_3	0.05493[b]	0.051[c]	0.046[d]
C_1-C_4	0.05872[b]	0.056[c]	0.057[d]
C_1-X_1	0.06589[b]	0.039[c]	0.031[d]
C_2-X_2		0.066[b]	
C_1-X_2	0.087[b]	0.087[b]	0.05[d]
C_2-X_3		0.056[c]	
C_1-X_3	0.08556[b]	0.061[c]	0.055[d]
C_2-X_4		0.086[b]	
C_1-X_4	0.08314[b]	0.083[b]	0.06[d]
C_2-X_5		0.074[c]	
X_1-X_2	0.1351[b]	0.11[e]	0.085[d]
X_1-X_3	0.11447[b]	0.076[c]	0.067[d]
X_2-X_4		0.114[b]	
X_1-X_4	0.10189[b]	0.08[e]	0.063[d]
f	1.4	1.5	2.1
$R/10^{-1}$	0.94 ± 0.03	1.60 ± 0.05	0.87 ± 0.03

[a] In this work the form factor has been calculated using the values of l_{ij} parameters reported from spectroscopic calculations[33] and from electron diffraction[34,35] in the gas phase, modified with a f factor (see text and expression 16). Distances r_{ij} and factor f were obtained by a least-squares fit minimizing an agreement factor R and are temperature independent within the accuracy displayed. [b] Reference 33. [c] Reference 34. [d] Reference 35. [e] This work. X = H (C_6H_6); X = F(C_6F_6); X_i = H($C_6H_3F_3$), i = 2, 4, 6; X_i = F($C_6H_3F_3$), i = 1, 3, 5.

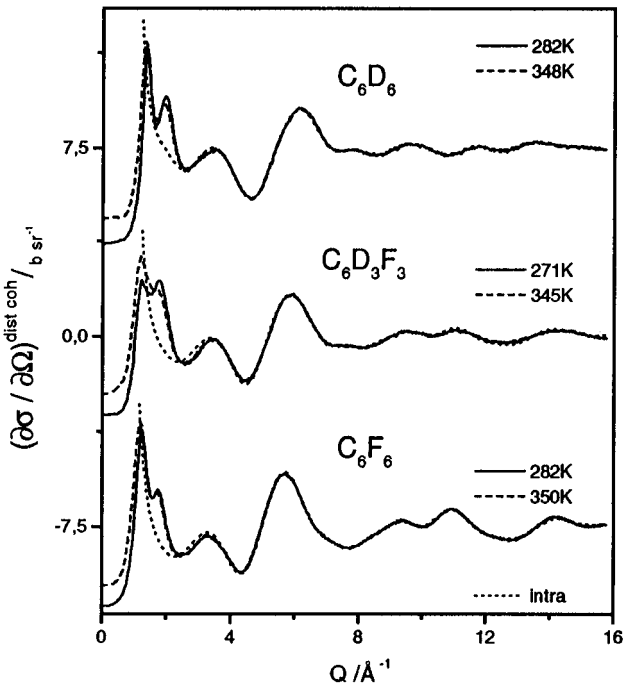

Figure 3. Coherent (distinct) cross section of liquid C_6D_6, 1,3,5-$C_6D_3F_3$, and C_6F_6 at the two extreme temperatures studied. The contribution of the calculated distinct intramolecular cross (temperature independent; see text and Table 2) is also reported. For clarity, curves are shifted: +7.5 for C_6D_6, −7.5 for C_6F_6.

range greater than 4 Å^{-1}, the predominant contribution comes from the distinct intramolecular cross section (eq 5) and appears as temperature independent. Hence in the temperature range investigated very small changes of the molecular parameters r_{ij} and l_{ij} (see eq 5) are expected. This intramolecular factor was estimated by fitting a calculated intramolecular cross section to the Q-weighted distinct cross section in the range 4−15.8 Å^{-1}. The fit was obtained by minimizing an agreement factor R defined as

$$R = \left(\frac{\sum_{Q_{min}}^{Q_{max}} Q^2 \left(\left(\frac{\partial\sigma}{\partial\Omega} \right)_{intra}^{dist} - \left(\frac{\partial\sigma}{\partial\Omega} \right)^{dist-coh} \right)^2}{\sum_{Q_{min}}^{Q_{max}} Q^2 \left(\left(\frac{\partial\sigma}{\partial\Omega} \right)^{dist-coh} \right)^2} \right)^{1/2} \quad (15)$$

where $(\partial\sigma/\partial\Omega)_{intra}^{dist}$ was evaluated in using three parameters for C_6D_6 and C_6F_6 and four parameters for $C_6D_3F_3$, respectively. These parameters are the distances r_{ij} and a parameter f used as a correcting factor to modify the Debye−Waller amplitudes according to the following relation:

$$l_{ij} = l_{ijtab} f \quad (16)$$

where l_{ijtab} are the values reported in Table 2. The initial parameters r_{ij} and l_{ij} (with $f = 1$) were taken from spectroscopic calculations[33] and from electron diffraction[34,35] in the gas phase, the final values of the parameters being given in Table 2. For 1,3,5-trifluorobenzene only the Debye−Waller amplitudes l_{ij} obtained from least-squares refinements are reported in the literature (associated to the distances C−C, C−F, and F−F[34]). Hence we have used values close to the analogous amplitudes in the benzene for *C−H* and *H−H* pairs. For l_{ij} parameters associated to the *H−F* distances a mean value of the corresponding Debye−Waller amplitudes in the C_6D_6 and C_6F_6 was used (see Table 2). The parameters r_{ij} and f fitted at different temperatures do not change within the accuracy displayed on the Table 2. In the temperature range investigated the agreement factor R varies somewhat (about 3%), as reported in Table 2. Clearly a good fit has been obtained using this procedure for C_6D_6 and C_6F_6 and only an acceptable one for $C_6D_3F_3$ (Figure 3).

The isothermal compressibility χ_T was obtained from the extrapolation, when Q approaches zero (see eq 6), of the differential coherent cross section $(\partial\sigma/\partial\Omega)^{coh}$ in fitting the low Q values (0.4−0.8 Å^{-1}) with a second-order polynomial. The values of χ_T obtained are presented in Table 3, and also as experimental thermodynamical values when available. It can be seen that the agreement obtained for C_6D_6 between these two sets of data (diffraction and thermodynamic) is good.

After removal of the contribution $(\partial\sigma/\partial\Omega)_{intra}^{dist}$ we have obtained $(\partial\sigma/\partial\Omega)_{inter}$ as a function of the temperature for the three neat liquids (Figure 4).

TABLE 3: Dependence upon the Temperature of the Isothermal Compressibility of Liquid Benzene, 1,3,5-Trifluorobenzene, and Hexafluorobenzene Obtained by Extrapolating Diffraction Data ($\chi_T/10^{-10}$ Pa^{-1}) (See Text)[a]

T/K	C_6H_6	$C_6H_3F_3$	C_6F_6
271		14.3	
282	9.0 (8.7)[b]		12.8
298	10.0 (9.7)[b]	15.5	14.5 (10.0)[c]
313			15.7
320			16.2
323	11.5 (11.9)[b]	17.1	
328			16.4
340			17.2
345		18.3	
348	13.5 (14.9)[b]		
350			18.2

[a] Experimental values obtained from thermodynamics[3,39] are also presented for comparison (in parentheses). [b] Reference 39. [c] Calculated from the thermodynamical value reported in ref 3.

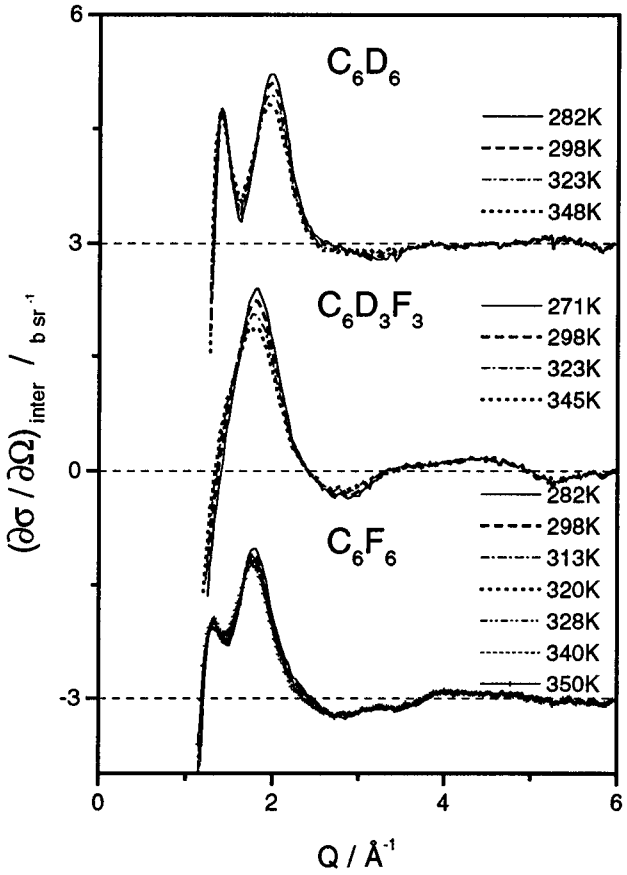

Figure 4. Dependence upon the temperature of the intermolecular cross section of the liquid C_6D_6, 1,3,5-$C_6D_3F_3$, and C_6F_6. For clarity, curves are shifted: +3 for C_6D_6, −3 for C_6F_6.

The intermolecular differential cross section of liquid benzene presents two well-defined peaks at about 1.4 and 2 Å^{-1} with different intensities and a barely visible feature at about 4 Å^{-1}. For liquid hexafluorobenzene, a similar trend is observed with two peaks detected at about 1.3 and 1.8 Å^{-1}, followed by an additional feature at about 4 Å^{-1} and which is slightly more pronounced than the corresponding one in C_6D_6.

In contrast, the general pattern for liquid 1,3,5-trifluorobenzene is rather different from the two previous ones. Indeed, a single broad and intense peak is detected at about 1.8 Å^{-1} and is accompanied by a weaker and broader feature which covers the range 3−5 Å^{-1}. It is noteworthy that the intense peak is at the same Q value that the stronger one observed in the C_6F_6. It comes out from these observations that the very short range order (3−5 Å^{-1}) in the 1,3,5-trifluorobenzene should be different than in the other two liquids. One might also infer that the intermediate range order should be rather similar for C_6D_6 and C_6F_6, as suggested by the existence of a first peak at about the same Q value (1.3−1.4 Å^{-1}). Finally at shorter range (1.6−2.0 Å^{-1}), the 1,3,5-$C_6D_3F_3$ and C_6F_6 should present a rather similar local order as indicated by the same peak centered at about 1.8 Å^{-1}.

If one considers now the temperature dependence of the diffraction patterns of the three liquids, it appears that the evolution is gradual upon heating along the coexistence curve from the melting point to the boiling point and remains rather small. Moreover, it must be pointed out that for the three compounds, it is in the Q domain corresponding to the stronger peak (about 1.8−2 Å^{-1}) that the temperature effect is the most significant.

For C_6F_6, a more detailed and extended study has been undertaken with special emphasis in the temperature domain centered at about 320 K, where an unusual structural behavior

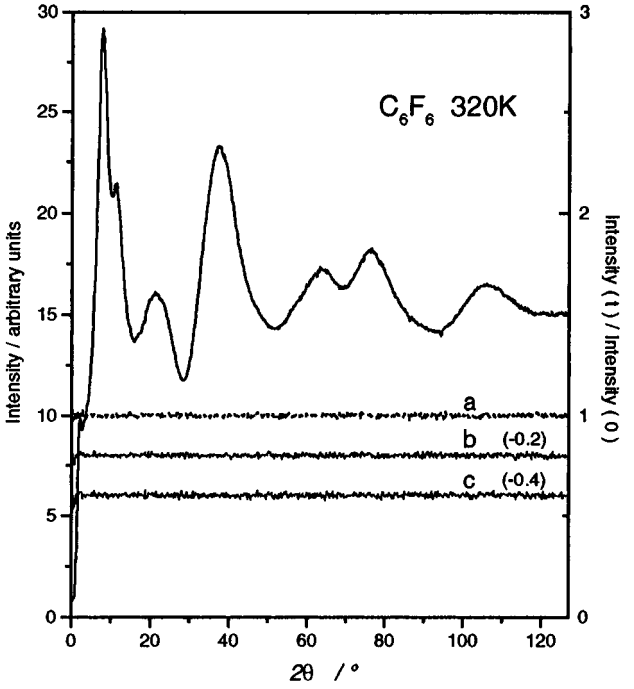

Figure 5. Experimental scattered intensities of liquid C_6F_6 at 320 K. Ratio of experimental intensities after 3 (a), 6 (b), and 9 h (c). For clarity, curves are shifted: −0.2 for (b), −0.4 for (c).

has been reported[16,17] as mentioned before (part I). We have found that the variation of the diffraction pattern is progressive and continuous without any unusual behavior upon heating in the corresponding temperature domain (Figure 4). In addition, it was also reported that without thermostating periods of at least 3 h the measurements were not reproducible. The usual procedure used in neutron-scattering experiments consists of accumulating, at a given temperature, several runs in order to improve the statistical accuracy; this allows us also to check easily any time-dependent effects, namely variation in the sample. The experimental intensities obtained at the temperature of 320 K, for which the most pronounced unusual structural behavior was reported, are presented in Figure 5. It is evident from Figure 5 that the ratio of the scattered intensities recorded after a time period of 3 h is equal to 1 (within an rms of 0.7%). The same conclusion is reached after 6 or 9 h (Figure 5). Therefore, the present neutron diffraction experiments give no indication which could corroborate the structural phenomena reported from depolarized light-scattering intensity measurements.[16,17]

The Fourier transform of the intermolecular differential cross section $(\partial\sigma/\partial\Omega)_{inter}$ (see expression 7) at the two extreme temperatures investigated is presented for the three systems in Figure 6. As the experimental momentum transfer range is limited (Q_{max} = 15.8 Å^{-1}) a modification function $M(Q) = j_0(\pi Q/Q_{max})$ was introduced in order to reduce the truncation effects.[1] The radial intermolecular pair correlation function $d_{inter}(r)$ of C_6D_6 and C_6F_6 show that the translational order involves at least two well-defined shells of neighboring molecules. In addition, it appears that this translational order is slightly more pronounced for C_6D_6 than for hexafluorobenzene. Whereas, for 1,3,5-$C_6D_3F_3$ the local order is less spatially extended than in the other two liquids, since the second shell of neighboring molecules is significantly damped. Moreover, in the first shell (4−9 Å), the packing is more visible in this liquid as evidenced by the wiggles observed in this region. This is better seen in the inset of Figure 6, where $d_{inter}(r)$ is presented in a more restricted range. The peak observed at about 4.4 Å for 1,3,5-$C_6D_3F_3$ smears out progressively upon heating. Notice also, as discussed before, that the evolution of the structure for all

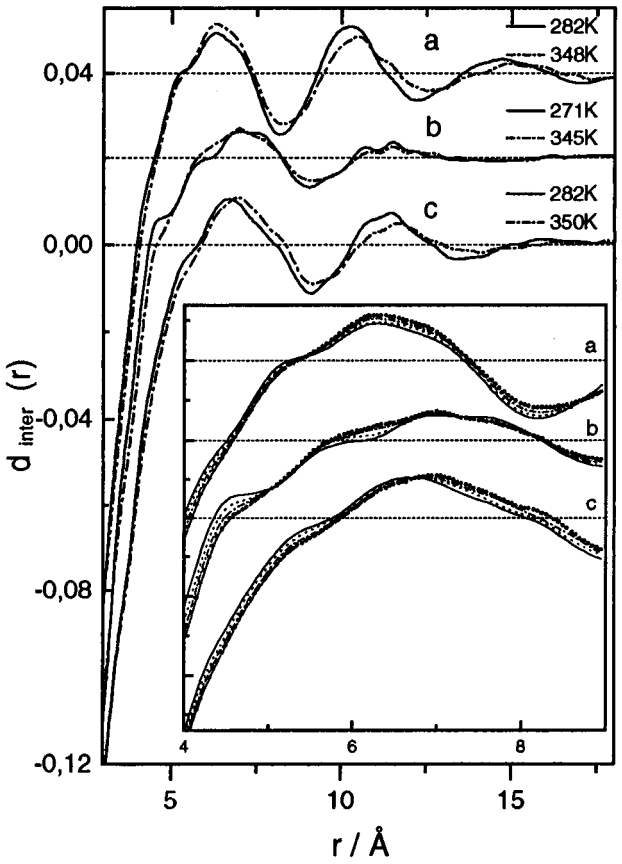

Figure 6. Intermolecular pair correlation function $d_{inter}(r)$ of the liquid C_6D_6 (a), 1,3,5-$C_6D_3F_3$ (b), and C_6F_6 (c) at the two extreme temperatures studied. A modification function $M(Q) = j_0(\pi Q/Q_{max})$, with $Q_{max} = 15.8\ Å^{-1}$, was used to reduce the truncation effects (see text and ref 1). For clarity, curves are shifted: +0.04 for C_6D_6, +0.02 for $C_6D_3F_3$. Detailed dependence upon the temperature in a restricted r range is presented in the inset: (—) 271 K for $C_6D_3F_3$, 282 K for C_6D_6 and C_6F_6; (···) 298 K; (-·-) 320 K for $C_6D_3F_3$, 323 K for C_6D_6 and C_6F_6; (-○-) 345 K for $C_6D_3F_3$, 348 K for C_6D_6, and 350 K for C_6F_6.

the three liquids, is progressive and continuous when the temperature increases.

Finally, the intermolecular correlation function $d(r^*)$ is presented as a function of a reduced distance $r^* = r/v_M^{1/3}$ (where $v_M = 1/\rho$, ρ being the number density) in Figure 7. This reduced unit r^* is used for convenience to account roughly of the size of the molecules. It appears that the $d(r^*)$ functions corresponding to C_6D_6 and C_6F_6 are similar to each other while in contrast, for 1,3,5-$C_6D_3F_3$, the $g(r^*)$ function is markedly different from the previous ones. In particular the first peak, centered at $r^* \cong 1.25$, is broader and asymmetric and presents a pronounced shoulder around $r^* \cong 1.05$.

V. Molecular Dynamics Simulation

1. Computational Details. The molecular dynamics simulations have been performed with *256* rigid molecules confined in a cubic cell of constant volume (microcanonical ensemble) and subjected to periodic boundary conditions. The equations of motion were solved using a leapfrog algorithm with a time step of 10^{-14} s and the molecular rotations were treated in the framework of the quaternion formalism. The cutoff radius of the intermolecular forces was equal to half of the box length, whereas long-range corrections corresponding to the repulsive and dispersive part of the potential were added to the pressure and potential energy. Each molecular dynamics run has needed 30×10^3 time steps after about 7.5×10^3 time steps of equilibration. We have chosen to use the Williams potential[37,38]

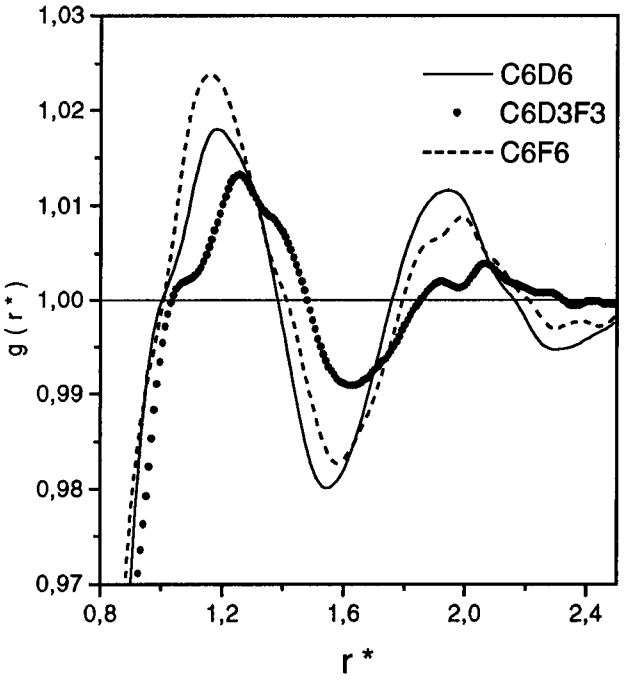

Figure 7. Comparison of the intermolecular pair correlation function $g_{inter}(r^*)$ of the liquid C_6D_6, 1,3,5-$C_6D_3F_3$, and C_6F_6 using reduced distances ($r^* = r/v_M^{1/3}$) at room temperature (see text).

TABLE 4: Intermolecular Potential Parameters Used in the Molecular Dynamics Simulations

potential parameters	C/Å^{-1}	B/kJ mol^{-1}	A/kJ Å^{-6} mol^{-1}
C−C	3.60	369 743	2439.8
F−F	4.35	400 000	500
H−H	3.74	11 971	136.4

to describe the intermolecular interactions in view of its ability to reproduce many properties of the liquid phase.[10,11] In this context, the intermolecular potential energy is given by a sum of atom−atom contributions:

$$U_{\alpha\beta}(r) = B_{\alpha\beta} \exp(-C_{\alpha\beta} r_{\alpha\beta}) - A_{\alpha\beta} r_{\alpha\beta}^{-6} + q_\alpha q_\beta r_{\alpha\beta}^{-1} \quad (17)$$

where α and β label the C, H, and F atoms and $r_{\alpha\beta}$ is the distance between the atoms α and β.

Values of the partial charges q are chosen to reproduce the experimental quadrupole moment of the molecule or are deduced from ab initio calculations while the cross potential parameters are calculated from the usual rules $B_{\alpha\beta} = (B_{\alpha\alpha}B_{\beta\beta})^{1/2}$, $C_{\alpha\beta} = {}^1/_2(C_{\alpha\alpha} + C_{\beta\beta})$, and $A_{\alpha\beta} = (A_{\alpha\alpha}A_{\beta\beta})^{1/2}$. The values of the latter potential parameters were originally determined from an energy minimization of the crystal structure[37,38] and are listed in Table 4. Furthermore the short-range intermolecular potential (i.e., the *A*, *B*, and *C* terms) for the F−F interactions has been modified from its original value[38] in order to obtain a better agreement with thermodynamical data, like vaporization heat,[39] for the liquid hexafluorobenzene at room temperature. As for the charge distributions on the benzene and on the hexafluorobenzene molecules they lead to values of the quadrupole moment in excellent agreement with those obtained from birefringence experiments[40] and are reported in Table 5. For the 1,3,5-trifluorobenzene, the short-range intermolecular potential (i.e., *A*, *B*, and *C* terms) is directly transferred from the benzene and hexafluorobenzene ones (Table 4). Nevertheless, the charge distribution on the 1,3,5-$C_6H_3F_3$ molecule is needed to determine the long-range electrostatic interactions. Therefore, to go further, two different procedures were used to model the electrostatic interactions in the 1,3,5-trifluorobenzene neat liquid. In the first one, we have followed an approach closely related

TABLE 5: Multipolar Constants and Point Charges Models

	C_6H_6	C_6F_6	$C_6H_3F_3$	
$Q_{zz}^{exp}/10^{-39}$ C m^2	−2.9[a]	+3.2[a]	+0.32[a]	
			model I	model II
$Q_{zz}^{MD}/10^{-39}$ C m^2	−2.8[b]	+3.2[b]	0.32	0.037
$\Omega_{YY}^{MD}/10^{-49}$ C m^3			−2.5	−11.9
q_C/au		+0.12[b]	+0.04727	+0.12
q_F/au		−0.12[b]	−0.03787	−0.12
$q_{C'}$/au	−0.153[b]		−0.02787	−0.153
q_H/au	+0.153[b]		+0.01846	+0.153

[a] Experimental values.[40] [b] From Williams model of atomic point charge.[37,38]

TABLE 6: Thermodynamical Properties (Potential Energy and Pressure) and Self-Diffusion Coefficient Obtained by MD Simulation of the Three Neat Liquids at Room Temperature (300 K)[a]

	d/kg m^{-3}	E_P/kg mol^{-1}	P/MPa	$D/10^{-9}$ m^2 s^{-1}
C_6H_6	872	−33.7 (−32.5)[b]	∼30 (<0.1)	1.2 (2.2)[d]
C_6F_6	1606	−32.7 (−33.3)[c]	∼80 (<0.1)	0.6
model I		−29.7	∼100	1.8
$C_6H_3F_3$	1267		(<0.1)	
model II		−30.6	∼100	1.6

[a] The experimental values are given in parentheses when available. For $C_6H_3F_3$ model I and II correspond, respectively, to parameters given in Table 5. [b] Reference 42. [c] Reference 43. [d] Reference 44.

to the one originally proposed by Williams.[37,38] We have performed ab initio calculations with molecular geometry optimization at the SCF energy level using a 6-311 G** basis set (GAUSSIAN 92 package) on the 1,3,5-$C_6H_3F_3$ monomer. The calculated values of the quadrupole and octopole moments are respectively $Q \sim +1.53\ 10^{-40}$ C m^2 and $\Omega \sim -6.1 \times 10^{-49}$ C m^3. The charges deduced from this calculation on the isolated monomer are then scaled using a simple multiplying factor in order to recover the experimental value of the quadrupole moment measured in an "inert" solvent (namely, liquid CCl_4). Moreover during this rescaling, we have taken into account the molecular geometry measured in condensed phase[34] instead of the geometry provided by the ab initio calculation. The values of the atomic charges are listed in Table 5. The intermolecular potential using this particular charge distribution will be referred as potential *I* in the following. Incidentally, let us recall that Fowler and Buckingham[41] have also proposed several sets of distributed atomic point charges for 1,3,5-$C_6H_3F_3$. However these charge distributions have been obtained for a weakly bonded $(1,3,5\text{-}C_6H_3F_3)_2$ dimer in a stacked conformation in gaseous phase.[41] Therefore their model of long-range intermolecular forces cannot be straightforwardly used here. In a second procedure (potential II), we have naively assumed that the charge distribution around the C−H and C−F bonds could be described directly by the atomic charges for benzene and hexafluorobenzene molecules and given by the Williams model (Table 5). Notice that the charge distributions used in potential I and II are quite different from each other. As for the thermodynamic states evaluated in our simulations, they correspond to those reported in Table 1. The accuracy reached by the MD calculations are presented in Table 6 the potential energy, the pressure and the self-diffusion coefficient obtained at room temperature for the three neat liquids. One notices that the pressure is systematically too high when the experimental density is used while the potential energy is close to the experimental one (a tendency known for benzene; see refs 7−11). Correspondingly the self-diffusion coefficient in simulated benzene is too small by a factor of roughly 2 as compared with experimental data. However a slight decrease of the simulated density is sufficient to improve the agreement with measured values at once for E_P, P, and D. Finally in the case of 1,3,5-trifluorobenzene the differences between models I and II are weak and are essentially significant on the potential energy, the greatest partial charges (model II) giving rise to the lowest energy.

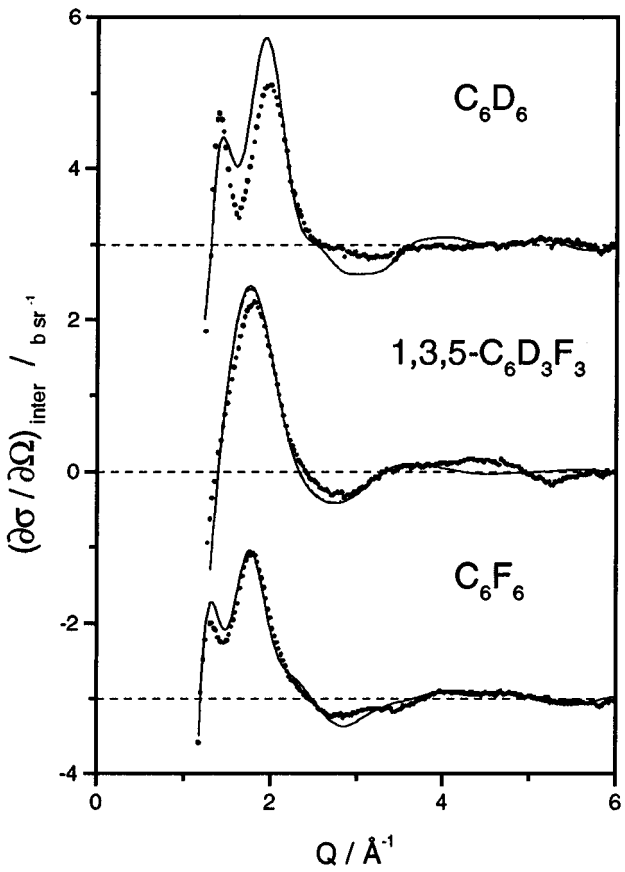

Figure 8. Comparison of the simulated (—) and experimental (···) intermolecular scattering cross section of the liquid C_6D_6, 1,3,5-$C_6D_3F_3$, and C_6F_6 at room temperature. For 1,3,5-$C_6D_3F_3$ model II (- - -) is also reported but is indistinguinshable from model I. For clarity, curves are shifted: +3 for C_6D_6, −3 for C_6F_6.

2. Comparison between Neutron Diffraction Data and Molecular Dynamics Results. As far as the comparison between neutron data and MD calculations for the intermolecular scattering cross section is concerned, the agreement is generally good as illustrated in Figure 8, although there is room for improvement. However, the experimental trends are well reproduced by the calculations in comparing liquid benzene and its fluorinated derivatives. Thus the position of the peaks as well as the spectacular absence of the first peak in 1,3,5-$C_6H_3F_3$ is reproduced successfully.

A comparison between calculated and experimental intermolecular pair correlation functions $g_{inter}(r)$ is reported in Figure 9a for liquid benzene at room temperature. We observe that the overall agreement is also satisfactory here, and we note in particular that the features existing at about 4, 5, and 6.2 Å, although weak, are correctly reproduced by the calculation. Notice that the same type of agreement between simulation results and experiment has already been pointed out in the literature (see refs 7 and 10).

The same overall agreement is still valid for C_6F_6 (Figure 9b) although slight discrepancies are now existing in the range 5.5−6.5 Å. In contrast, the overall agreement is not as good for 1,3,5-$C_6D_3F_3$ as for the other two liquids (Figure 9c). It must be pointed out that the use of potential II instead of potential I in the simulation leads to a pair correlation function which shows they are very close to each other and therefore does not change significantly the agreement with the experimental data (see Figure 9c).

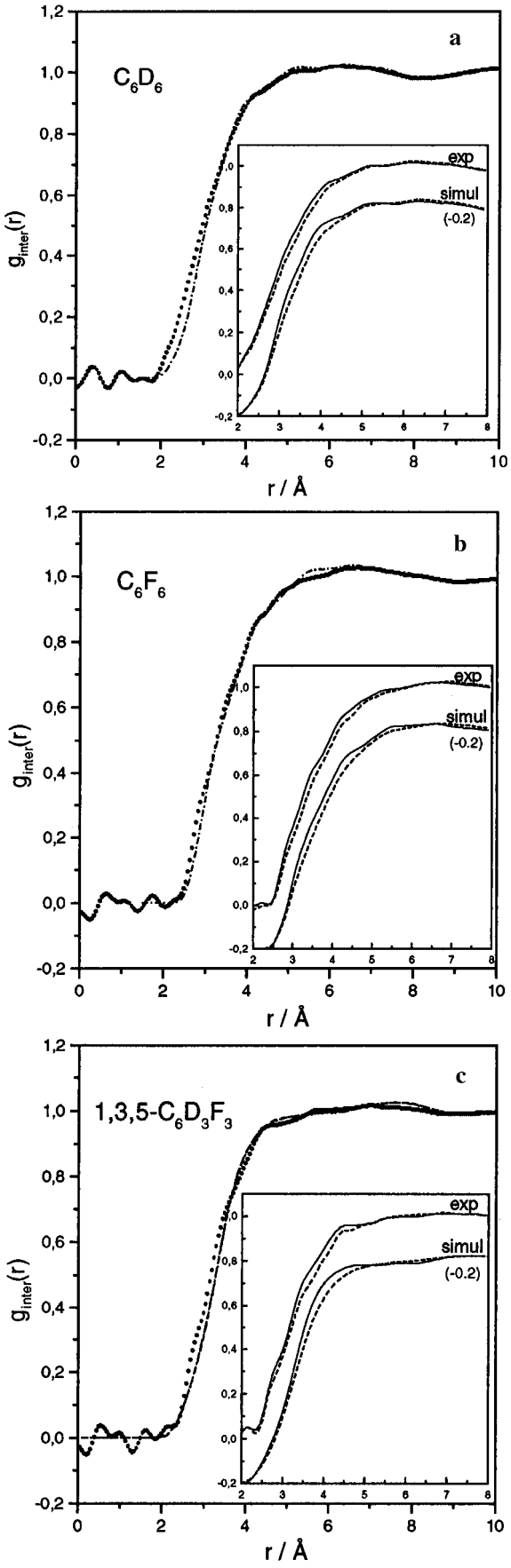

Figure 9. Comparison of the simulated (-·-) and experimental (···) intermolecular pair correlation function $g_{inter}(r)$ at room temperature. Comparison for the extreme temperatures studied is presented in the inset: (—) for temperature close to the melting point; (- - -) for temperature close to the boiling point. The simulated $g_{inter}(r)$ functions are shifted (−0.2): (a) liquid C_6D_6; (b) liquid C_6F_6; (c) liquid 1,3,5-$C_6D_3F_3$, model I (-·-), model II (- - -).

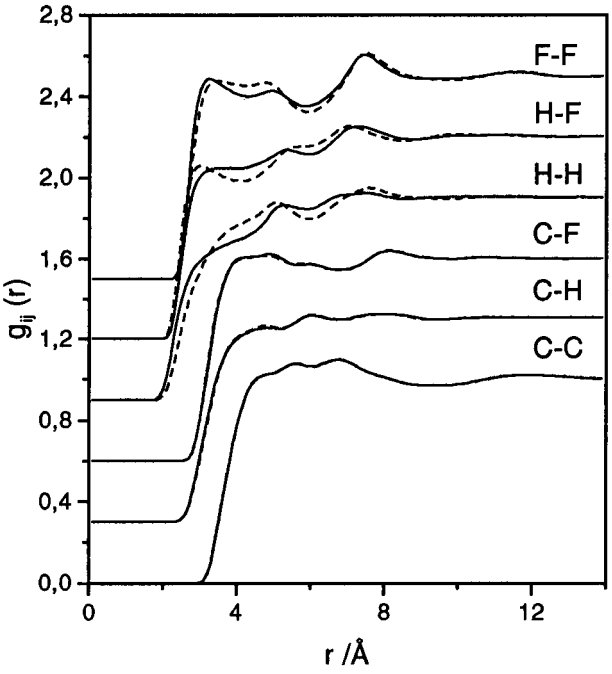

Figure 10. Atom−atom correlation function $g_{ij}(r)$ calculated from MD simulation of 1,3,5-$C_6H_3F_3$ using model I (—) and model II (- - -) (see text). For clarity, curves are shifted from each other (+0.3).

Let us emphasize that the calculated partial correlation functions $g_{ij}(r)$ for C−C, C−H, and C−F pairs using both potentials are almost identical, although the $g_{ij}(r)$ associated with H−H, H−F, and F−F pairs are rather different (see Figure 10). Nevertheless, their weighted average according to expression 11 leads to a total radial intermolecular correlation function $g_{inter}(r)$ which is almost model independent. This clearly shows that the uniqueness of a good potential to model the molecular interactions cannot be completely assessed only from the comparison of neutron diffraction experiments and molecular dynamics simulations. In this context, it is worthy reminding one that spectra obtained in collision-induced spectroscopy are useful to model the charge distribution.[13] Indeed the observed spectra are primarily governed by electrostatic interactions that are modulated by the density fluctuations. Although further improvement of the intermolecular potential should be carried out, the overall agreement using either potential I or II is sufficient to extract valuable structural information from the molecular dynamics simulation.

Finally the evolution of $g_{inter}(r)$ with the temperature is well reproduced by the simulation which confirms the weak variation of the local order in the three liquids between the melting point and the boiling point (see the insets of Figure 9a−c).

VI. Discussion

The discussion of the local order existing in the investigated liquids can be undertaken on the basis of the detailed information obtained from MD simulations and in particular in dealing with the partial pair correlation functions $g_{ij}(r)$ calculated for these systems. However, this analysis is made difficult when the molecules comprise many atoms. A more convenient approach is based upon the evaluation of the angular pair correlation function $G(r,\theta)$ defined as

$$\rho G(r,\theta) = (1/N)\langle \sum_{i \neq j}^{N} \delta(r - r_{ij})\delta(\theta - \theta_{ij})\rangle \qquad (18)$$

This function allows us to quantify the orientational correlations of a pair of molecules i and j having their center of mass

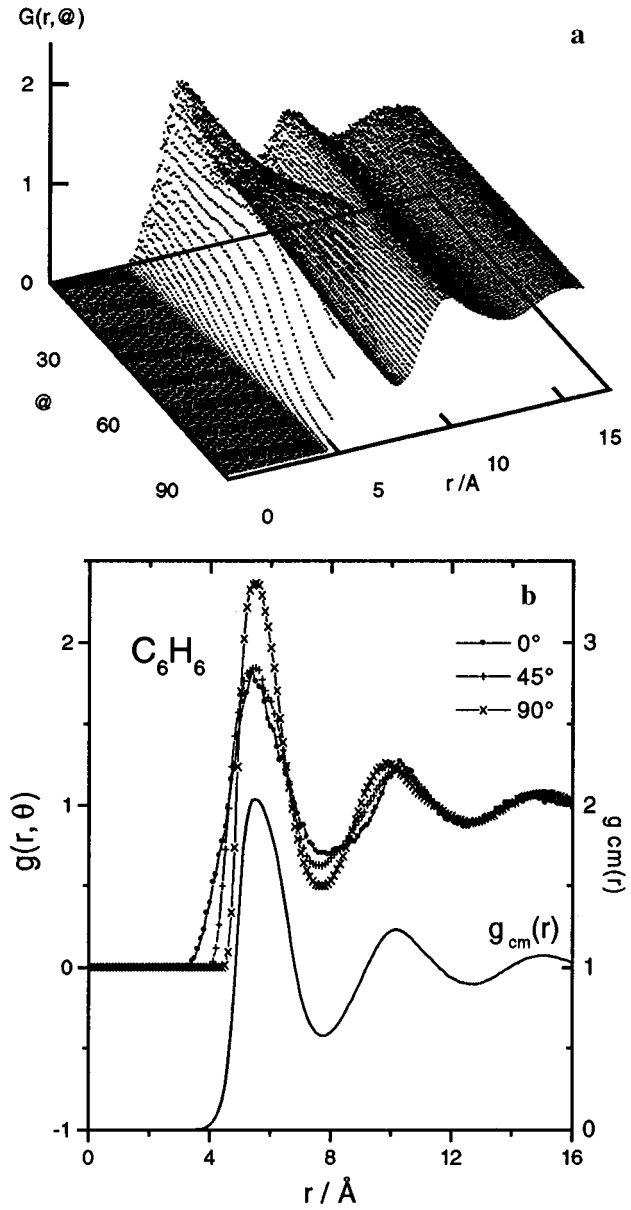

Figure 11. Pair correlation function of liquid C_6H_6 at room temperature: (a) radial and angular $G(r,\theta)$ function; (b) radial and angular function for θ equal to 0°, 45°, and 90°. Radial $g_{cm}(r)$ function of the center of mass is also reported.

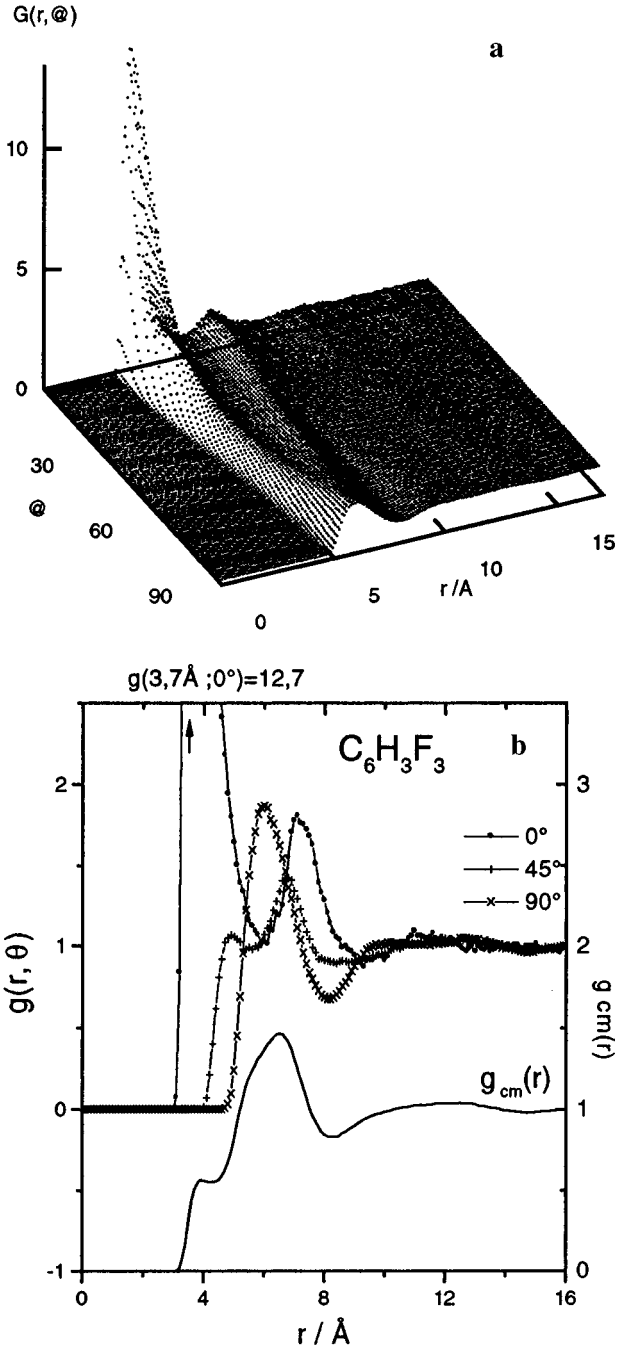

Figure 12. Pair correlation function of liquid $C_6H_3F_3$ at room temperature: (a) radial and angular $G(r,\theta)$ function; (b) radial and angular function for θ equal to 0°, 45°, and 90°. Radial $g_{cm}(r)$ function of the center of mass is also reported.

separated by a distance r_{ij} and where the angle between their main symmetry axes is θ_{ij}.

For illustration the evolution of the $G(r,\theta)$ function for liquid benzene is reported in Figure 11a. To understand more easily its behavior, we have considered three situations which are relevant to describe the orientational correlations in such liquids, namely parallel configurations ($\theta = 0°$), perpendicular configurations of molecular axes ($\theta = 90°$) and an intermediate configuration ($\theta \cong 45°$). The r dependence of the probability of occurrence of the parallel and perpendicular configurations shown in Figure 11b follows the same trend as that of the center of mass−center of mass distribution function, $g_{cm}(r)$, i.e., two maxima at about 5.5 and 10 Å, respectively separated by a minimum at about 8 Å. It should be emphasized that these considerations are also valid for the "intermediate" configuration ($\theta \cong 45°$). On average in liquid benzene no specific orientations of the molecules are privileged. This appears clearly on the more complete representation $G(r,\theta)$ (Figure 11a) where an almost complete isotropy is observed for distances greater than about 5 Å. However at distances less than 4.5 Å parallel configurations are favored for a better packing.

The structure of liquid 1,3,5-trifluorobenzene is quite different from the structure of the benzene. This conclusion comes out directly from the observation of the simulated $g_{cm}(r)$ (Figure 12b). Indeed, this function presents a very unusual shape with a well-defined prepeak at about 4 Å, followed by a broad intense peak at about 6.5 and a smeared out one at larger distances (10−14 Å) corresponding to the second shell of neighbors. Clearly, a well-defined structure is present in the range 3.5−4.5 Å and has no counterpart in liquid benzene (for a preliminary account see ref 15). In examining $G(r,\theta)$ presented in Figure 12a the first remarkable feature concerns the region close to 4 Å where a stacked structure of molecules comes out. Parallel configurations are again favored at $r \cong 7.5$ Å slightly after the position of the main peak in the $g_{cm}(r)$ function (see Figure 12b). For the perpendicular configuration a maximum is observed at about 6 Å, just before the first maximum of $g_{cm}(r)$.

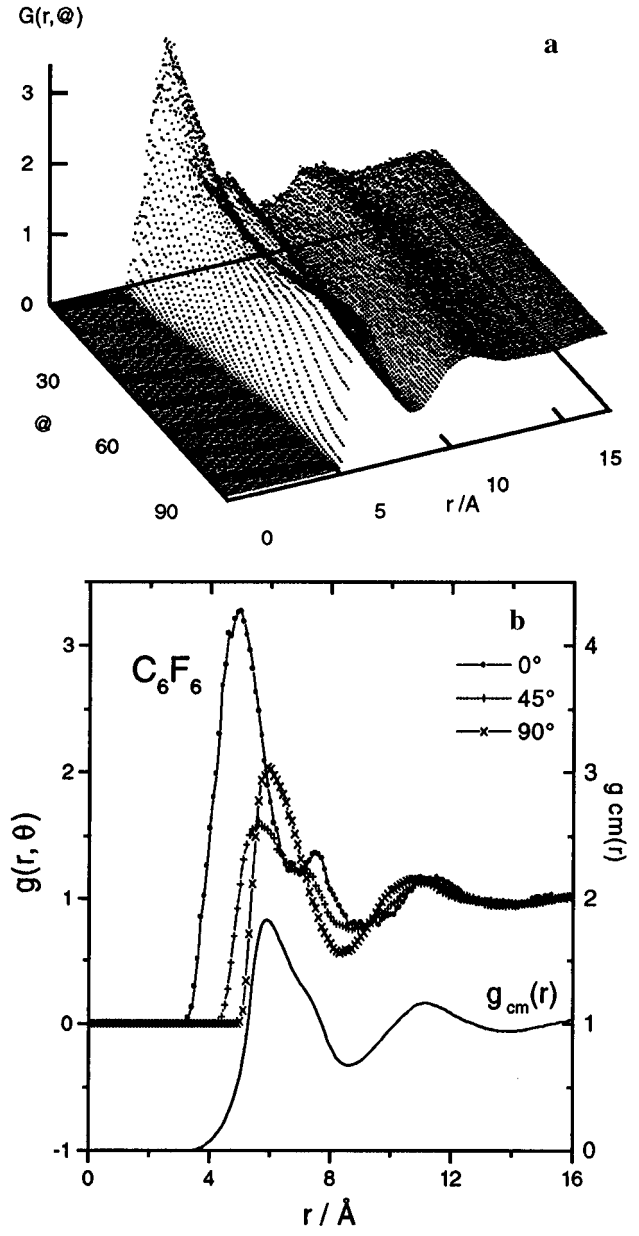

Figure 13. Pair correlation function of liquid C_6F_6 at room temperature: (a) radial and angular $G(r,\theta)$ function; (b) radial and angular function for θ equal to 0°, 45°, and 90°. Radial $g_{cm}(r)$ function of the center of mass is also reported.

Hence the broad and asymmetrical shape of the main peak of $g_{cm}(r)$ in liquid 1,3,5-trifluorobenzene is related to these perpendicular and parallel configurations of molecules which have their maxima of occurrence for different values of r. This situation contrasts with the one reported for benzene, for which the observed symmetry of the first peak of $g_{cm}(r)$ results from the fact that parallel and perpendicular configurations of molecules have their maxima located at the same r values (isotropy). Finally let us emphasize that the second shell of neighbors is strongly damped as compared with that exhibited by liquid benzene. This observation may be interpreted as a consequence of the out of phase distribution between parallel and perpendicular configurations existing in 1,3,5-trifluorobenzene.

In liquid hexafluorobenzene the analysis of the $G(r,\theta)$ function (Figure 13a) shows that parallel configurations are rather dominant at short distances. More precisely $G(r,\theta=0°)$ presents a first maximum close to 5 Å while perpendicular configurations characterized by $G(r,\theta=90°)$ present a maximum around $r \sim 6$ Å (Figure 13b). If we follow the same rationale than previously, it might be inferred that the low-r flank of the first peak of $g_{cm}(r)$ is related to the existence of parallel configurations whereas its high-r flank originates from perpendicular and intermediate configurations. Moreover, the second maximum shown by $G(r,\theta=0°)$ (parallel configurations) at 7.5 Å is responsible for the shoulder observed in the $g_{cm}(r)$ in this region.

Let us recall (as we have pointed out before, in section I) that at room temperature for liquid benzene[2−6] and for hexafluorobenzene[3,4] previous results had put in evidence the existence of favored perpendicular configurations.

An important point of this study concerns the existence of a well-defined dimer in 1,3,5-trifluorobenzene. To substantiate this point, we have calculated the number of neighboring molecules n in a spherical shell around a central molecule. For liquid 1,3,5-trifluorobenzene, the radius of the shell was fixed at a value of 4.8 Å (reduced distance $r^* = 0.86$) associated with the prepeak in $g_{cm}(r)$ (see also $G(r,\theta=0°)$ in Figure 12b) and n was found to be close to 1. This result establishes that almost all pairs of molecules in close contact form a stacked structure in the liquid phase.

In contrast, for liquid benzene and hexafluorobenzene, the values of n were found to be 0.15 and 0.42, respectively, for distances of 4.6 and 5.0 Å, which correspond to the previous reduced distance $r^* = 0.86$. This result is consistent with the absence of a prepeak in $g_{cm}(r)$ associated with these two liquids. Hence, we can conclude that the dimers observed in liquid 1,3,5-trifluorobenzene do not exist in the two other liquids. Notice that the existence of dimers in liquid state has been recently reported.[45] Let us emphasize that all the above features are only weakly affected upon heating (between T_{mp} and T_{bp}).

To give a tentative explanation of the structural differences exhibited by the three liquids in terms of the geometry and intermolecular potential of the molecules, the following simplified picture can be considered. The ordering in liquid 1,3,5-trifluorobenzene at short separation is that expected if only short-range forces (especially the electrostatic ones) are operating. The less trivial behavior of the other two liquids (only a small occurrence of stacked configuration at short separation) is a consequence of a delicate balance between steric effect and quadrupole-quadrupole interactions for a better packing at liquid density. Thus the similar magnitude of the quadrupole moment of C_6H_6 and C_6F_6 (the quadrupole−quadrupole interaction favors perpendicular arrangement) and the smaller cross section of C_6H_6 (hydrogen atoms are smaller than fluorine atoms) permits us to understand the reduction of the fraction of parallel arrangement in liquid benzene as compared to liquid hexafluorobenzene.

VII. Conclusion

The evolution of the structure in the three neat liquids benzene, hexafluorobenzene, and 1,3,5-trifluorobenzene was investigated as a function of the temperature from the melting point up to the boiling point, combining neutron diffraction experiments and molecular dynamics simulations. It was found that the variation of the local order was progressive and remains small upon heating for all the three liquids. In particular for hexafluorobenzene neutron diffraction experiments as well as MD simulations do not corroborate the "structural transition" reported from light-scattering measurements.[16,17]

The overall good agreement obtained between the simulated and the experimental pair correlation functions has allowed us to study the orientational order in the two first shells of neighbors using the results provided by MD simulations. We have adopted an approach based upon the analysis of the angular pair correlation function $G(r,\theta)$ describing the probability

distribution of the relative orientation θ between the main symmetry axes of a pair of molecules separated by a distance r. Two extreme situations, namely, parallel and perpendicular configurations of the molecules have been more specifically considered.

For liquid benzene we find that the probability of occurrence of the perpendicular and parallel configurations present the same behavior with r as the center of mass−center of mass distribution function $g_{cm}(r)$, i.e., their successive maxima and minima are in phase with each other and with the ones of the $g_{cm}(r)$.

For liquid hexafluorobenzene, although perpendicular and parallel configurations occur in the first shell as in benzene, they appear at different distances (out of phase), with close contact favoring parallel configurations, while perpendicular configurations are shifted more outward. As a consequence a shoulder on the high-r flank of the first peak of $g_{cm}(r)$ is observed for hexafluorobenzene.

For liquid 1,3,5-trifluorobenzene the orientational order is very different from that of liquid benzene and is more reminiscent of that found in hexafluorobenzene. However a well-defined structure of molecules appears at short distances $r \leq 4.5$ Å, suggesting the presence of sandwichlike dimers. Furthermore, it is found that perpendicular configurations appear only above 5 Å. This redistribution is responsible of the unusual shape exhibited by the first peak of the $g_{cm}(r)$ function and of the disappearance of the first peak in the intermolecular scattering cross section.

Finally, although in the three liquids the analysis based on $G(r,\theta)$ points out that parallel configurations of molecules are always favored at very short distances, the number of molecules involved in this type of configuration is only significant (i.e., close to one) for liquid 1,3,5-trifluorobenzene. This finding explains the markedly different intermolecular structure factor of $C_6D_3F_3$ probed by neutron-scattering experiment as compared with those of the other two liquids (C_6D_6 and C_6F_6) and leads to the conclusion that on the time scale involved in neutron diffraction experiments a (1,1) sandwichlike complex exists in liquid 1,3,5-trifluorobenzene between the melting point and the boiling point.

As a final conclusion it is interesting to remark that values of physical quantities associated with these molecules, such as molar mass, volume, and quadrupole moment, could lead to classify 1,3,5-trifluorobenzene between benzene and perfluorinated benzene. This study shows that structurally it is in fact the perfluorinated molecule which should be placed between benzene and 1,3,5-trifluorobenzene.

Acknowledgment. The authors are indebted to Mrs. N. Ratovelomanana and M. F. Lautier (L.A.S.I.R., UPR 2631, Thiais, France) for the synthesis of the deuterated 1,3,5-trifluorobenzene. The authors are pleased to gratefully acknowledge M.-C. Bellissent-Funel for her valuable help with the neutron diffraction experiments and wish to thank Mr. J. P. Ambroise (L.L.B., C.N.R.S.-C.E.N., Saclay) for his technical assistance during the experiments. M.B. and M.I.C. acknowledge the Ministère des Affaires Etrangères (France) and the I.N.I.C. (Portugal) for Grant 44100 under the auspice of which this work has been performed. Finally we acknowledge the IDRIS (CNRS, Saclay) and the MASTER of the ENSPCB (Université de Bordeaux I) for allocation of computer time.

References and Notes

(1) Cabaço, M. I.; Danten, Y.; Besnard, M.; Bellissent-Funel, M.-C.; Guissani, Y.; Guillot, B. *Mol. Phys.* **1997**, *90*, 817.

(2) Narten, A. H. *J. Chem. Phys.* **1968**, *48*, 1630; **1977**, *67*, 2102.

(3) Bartsch, E.; Bertagnolli, H.; Schulz, G.; Chieux, P. *Ber. Bunsen-Ges. Phys. Chem.* **1985**, *89*, 147.

(4) Bartsch, E.; Bertagnolli, H.; Chieux, P. *Ber. Bunsen-Ges. Phys. Chem.* **1986**, *90*, 34.

(5) Felici, R.; Cilloco, F.; Bosi, P. *Mol. Phys.* **1990**, *70*, 455.

(6) Misawa, M.; Fukunaga, T. *J. Chem. Phys.* **1990**, *93*, 3495.

(7) Steinhauser, O. *Chem. Phys.* **1982**, *73*, 155.

(8) Linse, P. *J. Am. Chem. Soc.* **1984**, *106*, 5425. Linse, P.; Engstrom, B.; Jonsson, B. *Chem. Phys. Lett.* **1985**, *115*, 95.

(9) Anderson, J.; Ullo, J. J.; Yip, S. *J. Chem. Phys.* **1987**, *86*, 4078.

(10) Yashonath, S.; Price, S. L.; Mc Donald, I. R. *Mol. Phys.* **1988**, *64*, 361.

(11) Danten, Y; Guillot, B.; Guissani, Y. *J. Chem. Phys.* **1992**, *96*, 3782.

(12) Steed, J. M.; Dixon, T. A.; Klemperer, W. *J. Chem. Phys.* **1979**, *70*, 4940.

(13) Besnard M.; Danten, Y.; Tassaing, T. In *Collision-and-Interaction Induced Spectroscopy;* NATO ASI Series C; Tabisz, G. C., Neuman, M. N., Eds.; Kluwer Academic Publishers: Dordrecht, 1995; Vol. 452, p 201.

(14) Del Campo, N.; Besnard, M.; Yarwood, J. *Chem. Phys.* **1990**, *142*, 91.

(15) Cabaço, M. I.; Danten, Y.; Besnard, M.; Guissani, Y.; Guillot, B. *Chem. Phys. Lett.* **1996**, *262*, 120.

(16) Rozhdestvenskaya, N. B.; Smirnova, L. V. *JETP Lett.* **1986**, *44*, 168.

(17) Rozhdestvenskaya, N. B.; Smirnova, L. V. *J. Chem. Phys.* **1991**, *95*, 1223.

(18) Grubbs, W. T.; MacPhail, R. A. *J. Phys. Chem.* **1992**, *96*, 8688.

(19) Cabaço, M. I.; Danten, Y.; Besnard, M.; Guissani, Y.; Guillot, B., to be published.

(20) Ambroise, J.-P.; Bellissent-Funel, M.-C; Bellissent, R. *Rev. Phys. Appl. A* **1984**, *19*, 731.

(21) Bertagnolli, H.; Chieux, P.; Zeidler, M. D. *Mol. Phys.* **1976**, *32*, 759.

(22) Paalman, H. H.; Pings, C. J. *J. Appl. Phys.* **1962**, *33*, 635.

(23) Blech, I. A.; Averbach, B. L. *Phys. Rev.* **1965**, *137*, A1113.

(24) Yaws, C. L.; Turnbough, A. C. *Chem. Eng.* **1975**, *Sept 1*, 107.

(25) Perry, J. H. *Chemical Engineer's Handbook*; McGraw Hill: New York, 1963; pp 3−273.

(26) Placzek, G. *Phys. Rev.* **1952**, *86*, 377.

(27) Powles, J. G. *Adv. Phys.* **1973**, *22*, 1. Rickayzen, G.; Powles, J. G. *Mol. Phys.* **1976**, *32*, 301. Powles, J. G.; Rickayzen, G. *Mol. Phys.* **1976**, *32*, 323.

(28) Blum, L.; Narten, A. H. *J. Chem. Phys.* **1976**, *64*, 2804. Blum, L.; Rovere, M.; Narten, A. H. *J. Chem. Phys.* **1982**, *77*, 2647.

(29) Egelstaff, P. A.; Soper, A. K. *Mol. Phys.* **1980**, *40*, 553, 569.

(30) Damay, P.; Leclercq, F.; Chieux, P. *Phys. Rev. B* **1990**, *41*, 9676.

(31) Bellissent-Funel, M.-C.; Bosio, L.; Teixeira, J. *J. Phys. Condens. Matter* **1991**, *3*, 4065.

(32) Bausenheim, T.; Bertagnolli, H.; Todheide, K.; Chieux, P. *Ber. Bunsen-Ges. Phys. Chem.* **1991**, *95*, 577.

(33) Cyvin, S. J. *Molecular Vibrational and Mean Square Amplitudes;* Amsterdam: Elsevier: 1968; p 245.

(34) Almenningen, A.; Hargitai, I.; Brunvoll, J.; Domenicano, A.; Samdal, S. *J. Mol. Struct.* **1984**, *116*, 199.

(35) Almenningen, A.; Bastiansen, O.; Seip, R.; Seip, H. M. *Acta Chem. Scand.* **1964**, *18*, 2115.

(36) Sears, V. F. *International Tables for Crystallography*; Wilson, A. J. C., Ed.; Kluwer Academic Press: Dordrecht, 1992; Vol. C, p 384.

(37) Williams, D. E.; Cox, S. R. *Acta Crystallogr.* **1984**, *B40*, 404.

(38) Williams, D. E.; Houpt, D. J. *Acta Crystallogr.* **1986**, *B42*, 286.

(39) *Handbook of Chemical and Physics*; Lide, D. R., Ed.; CRC Press: Boca Raton, FL, 1995.

(40) Gray, C. G.; Gubbins, K. E. *Theory of Molecular Fluids;* Clarendon Press: Oxford, 1984.

(41) Fowler, P. W.; Buckingham, A. D. *Chem. Phys. Lett.* **1991**, *176*, 11.

(42) Ben Naim, A.; Marcus, Y. *J. Chem. Phys.* **1984**, *81*, 2016.

(43) Counsell, J. F.; Green, J. H. S.; Halls, J. L.; Martin, J. F. *Trans. Faraday Soc.* **1965**, *61*, 212.

(44) Falcone, D. R.; Douglass, D. C.; McCall, D. W. *J. Phys. Chem.* **1967**, *71*, 2754.

(45) Howe, M. A.; Wormald, C. J.; Neilson, G. W. *Mol. Phys.* **1989**, *66*, 847.